The Relationship between Sea Surface Temperature and Maximum Intensification Rate of Tropical Cyclones in the North Atlantic

JING XU

State Key Laboratory of Severe Weather, Chinese Academy of Meteorological Sciences, China Meteorological Administration, Beijing, China

YUQING WANG

International Pacific Research Center, and Department of Atmospheric Sciences, University of Hawai'i at Mānoa, Honolulu, Hawaii

ZHE-MIN TAN

Key Laboratory of Mesoscale Severe Weather, Ministry of Education, and School of the Atmospheric Sciences, Nanjing University, Nanjing, China

(Manuscript received 30 May 2016, in final form 31 July 2016)

ABSTRACT

An empirical relationship between sea surface temperature (SST) and the maximum potential intensification rate (MPIR) of tropical cyclones (TCs) over the North Atlantic has been developed based on the best-track TC data and the observed SST during 1988–2014. Similar to the empirical relationship between SST and the maximum potential intensity of TCs previously documented, results from this study show a nonlinear increasing trend of the MPIR with increasing SST, with a more rapid increasing trend when SST is higher than 27°C. Further analyses indicate that about 28% of intensifying TCs over the North Atlantic reached 50% of their MPIR and only 7% reached 80% of their MPIR at the time when they were at their lifetime maximum intensification rates. Moreover, a TC tended to have a larger intensification rate when it was located in regions with higher SST and lower vertical wind shear (VWS). This indicates that although the MPIR–SST relationship is much stronger than that for the IR rate versus SST for most TCs, the actual intensification rate of a TC is determined by not only the SST but also other environmental effects, such as VWS. Additional results from a simplified dynamical system previously developed for TC intensity prediction suggest an SST-dependent TC MPIR, similar to that fitted from observations. However, the MPIR obtained from the observational fitting seems to underestimate the MPIR in regions with low SST at higher latitudes where VWS is often large. Nevertheless, this study provides the observational evidence for the existence of the MPIR for TCs.

1. Introduction

Tropical cyclones (TCs) form over warm tropical oceans with high sea surface temperature (SST) and a deep mixed layer, a moist middle to lower troposphere, and weak vertical wind shear (Gray 1968). TCs get energy from the underlying ocean in the form of surface entropy flux, which is largely determined by SST. Therefore, SST is a key factor to the formation and intensification of TCs (Malkus and Riehl 1960) and largely determines the maximum potential intensity (MPI) that a TC can achieve given favorable environmental atmospheric and oceanic conditions (Miller 1958; Emanuel 1986, 1988, 1997; Holland 1997).

Miller (1958) developed the first relationship between SST and the TC maximum intensity in terms of the minimum sea level pressure (SLP) based on the surface pressure decrease resulting from warming due to lifting surface air moist adiabatically to near the tropopause in the eyewall and then subsiding dry adiabatically back to the surface in the eye. In this simple theoretical framework, to attain realistic relative humidity in the eye, some mixing with air in the eyewall during the subsidence must be included. Emanuel (1986, 1988, 1991, 1995, 1997)

Corresponding author address: Prof. Yuqing Wang, Room 404A, IPRC/SOEST, University of Hawai'i at Mānoa, 1680 East-West Road, Honolulu, HI 96822.
E-mail: yuqing@hawaii.edu

DOI: 10.1175/JAS-D-16-0164.1

developed an MPI theory (E-MPI) based on the assumption that a TC can be treated as a Carnot heat engine (Kleinschmidt 1951). The E-MPI in terms of the minimum SLP (Emanuel 1986, 1988) or the maximum near-surface wind speed (Emanuel 1995, 1997) is a function of the underlying SST, the ambient near-surface air temperature and relative humidity, and the outflow-layer temperature in the upper troposphere. Nevertheless, because of the strong dependence of the outflow-layer temperature on the SST and the fairly uniform relative humidity over the tropical/subtropical oceans (Emanuel 1988), the E-MPI can be considered as a function of SST only to the first approximation. Actually, both Miller (1958) and Emanuel (1988) predicted an increase of the MPI with increasing SST.

The relationship between SST and the TC maximum intensity has also been empirically established from observations based on climatological SST data (Merrill 1988; DeMaria and Kaplan 1994) for North Atlantic TCs. Both E-MPI and the empirically determined relationships between SST and the MPI have been used in statistical TC intensity forecast schemes (DeMaria and Kaplan 1994; DeMaria et al. 2005). The empirically determined MPI is easily obtained routinely based on the observed SST or the climatological SST. In sharp contrast, the theoretical MPI needs various assumptions, such as a constant air–sea temperature difference (e.g., 1°C in most applications) and a fixed ambient surface relative humidity (often taken as 80%), while both may vary considerably under TC conditions in reality.

Although the MPI as a function of SST has been well established both theoretically and empirically, it is unknown whether a similar relationship between SST and the maximum potential intensification rate (MPIR) of TCs exists given favorable environmental conditions, similar to the MPI. In this study, we attempt to address this issue based on observations for North Atlantic TCs in a similar way as that used in DeMaria and Kaplan (1994). We hypothesize that the SST not only determines the MPI but also the MPIR of TCs. As a result, a similar relationship between SST and the MPIR exists and can also be empirically determined. The data and analysis methods are described in section 2. Section 3 presents the analysis of the relationship between SST and the IR (and MPIR) for North Atlantic TCs and the construction of a new empirical MPIR as a function of SST. The SST dependence of MPIR in a simplified dynamical system previously developed for TC intensity prediction is briefly discussed in section 4. Main conclusions will be drawn in the last section.

2. Data and methodology

The best-track data (HURDAT2) of North Atlantic TCs during 1988–2014 were obtained from the National Hurricane Center (NHC; available online at http://www.nhc.noaa.gov/data/#hurdat). HURDAT2 consists of 6-hourly TC center position (latitude and longitude), maximum 1-min-mean sustained surface wind speed V_{max}, central SLP, and so on. All extratropical transition stages and records after landfall were removed from our analysis to allow us to focus on the MPIR. The intensification rate (IR) of a TC at a given time was defined as the following 24-h V_{max} increase. Therefore, the weakening with IR less than zero was not included in the analysis. A total of 343 TCs and 4066 intensifying cases were included in this study.

The high-resolution SST product of the National Oceanic and Atmospheric Administration (NOAA) optimum interpolation sea surface temperature (OISST), version 2 (Reynolds et al. 2007), was used in this study and was obtained from ftp://eclipse.ncdc.noaa.gov/pub/OI-daily-v2/climatology/. The high-temporal- and high-spatial-resolution OISST product was blended with in situ data and satellite data and given daily on 0.25° × 0.25° grids since 1988, which has been widely used in TC research in recent years (e.g., Chen et al. 2015; Murakami et al. 2015). This high-resolution SST data can better reflect the cold wake following a TC track and thus is suitable for the study of TC intensity change. The OISST SST was averaged within a radius of 1° latitude for each TC case in our analysis.

Following Emanuel et al. (2004), we subtracted 40% of the translational speed from the maximum sustained wind speed of each TC record when we evaluate the relationships between SST and the TC MPI and between SST and the TC IR. The translational speed of a TC at a given time was calculated using the centered time differencing based on changes in latitude and longitude at 6-h intervals, except for the first and the last two records where one-sided time differencing was used. Note the difference from DeMaria and Kaplan (1994) and Zeng et al. (2007), who subtracted 100% of the translational speed from V_{max}, which might be unrealistic for fast-moving, weak TCs. To establish the relationship between SST and TC IR, following DeMaria and Kaplan (1994) and Zeng et al. (2007), each TC observation was assigned to an SST bin. The SSTs from 22° to 31°C were divided into nine evenly spaced bins, each in 1°C intervals as indicated in Table 1.

The European Centre for Medium-Range Weather Forecasts (ECMWF) interim reanalysis (ERA-Interim) data were used to calculate vertical shear of large-scale environmental wind (VWS) in this study. The ERA-Interim data used in this study have horizontal resolution of 0.75° in both longitude and latitude on 37 pressure levels at 6-h intervals. The VWS in this study was calculated following the method described

TABLE 1. Numbers of intensifying TC cases (percentage of total in parentheses), the averaged IR of all cases, and the averaged IR of the top-50% IR cases, numbers of TCs (percentage of total in parentheses), and the corresponding values for the lifetime maximum IR (IR_{max}) of intensifying TCs in given SST groups in the North Atlantic during 1988–2014.

SST midpoint (°C)	Number of intensifying TC cases (%)	Averaged IR (kt day^{-1})	Averaged IR of the top-50% IR (kt day^{-1})	Number of intensifying TCs (%)	Averaged lifetime IR_{max} (kt day^{-1})	Averaged IR of the top-50% lifetime IR_{max} (kt day^{-1})
(20, 21]	5 (0.1)	5.7	8.5	1 (0.3)	9.5	9.5
(21, 22]	26 (0.6)	3.8	5.9	2 (0.6)	9.6	11.9
(22, 23]	54 (1.3)	8.0	12.0	4 (1.2)	17.6	25.0
(23, 24]	70 (1.7)	7.3	12.4	6 (1.8)	15.9	21.4
(24, 25]	120 (3.0)	8.4	13.5	11 (3.2)	18.3	26.4
(25, 26]	266 (6.5)	8.8	14.6	15 (4.6)	15.9	20.7
(26, 27]	653 (16.1)	12.3	19.8	38 (11.1)	25.0	35.4
(27, 28]	1192 (29.3)	13.3	21.4	107 (31.3)	24.3	34.7
(28, 29]	1246 (30.6)	14.6	23.5	106 (31.0)	25.4	36.9
(29, 30]	409 (10.1)	17.8	28.0	49 (14.0)	28.5	42.1
(30, 31]	25 (0.6)	15.6	27.8	4 (1.2)	27.8	44.6

in Wang et al. (2015). First, the large-scale horizontal winds were calculated using the filtering algorithm of Kurihara et al. (1993), which removed all disturbances, including TCs, with wavelengths less than 1000 km. Then, the VWS was calculated as the difference in vector winds between 200 and 850 hPa averaged within a 1000-km radius from the TC center. Note that the use of a smaller radius provided similar results since the filtering was applied before the calculation of the area average (Wang et al. 2015).

3. TC intensity and IR versus SST

a. TC intensity versus SST

Before we discuss the TC IR and the MPIR, we first briefly discuss the relationship between SST and the MPI over the North Atlantic during our study period. Several previous studies have established empirical relationships between SST and the MPI for North Atlantic TCs (DeMaria and Kaplan 1994; Zeng et al. 2007, 2008) but based on different SST datasets and different time periods. DeMaria and Kaplan (1994) used the climatological monthly mean SST data and TC data during 1962–92 while Zeng et al. (2007, 2008) used the weekly coarse (1° × 1°)-resolution Reynolds SST data (Reynolds et al. 2002) for TCs during 1981–2003. Figure 1 shows the scatter diagram of intensity in terms of maximum sustained near-surface wind speed V_{max} versus SST for all TC cases during 1988–2014 in the North Atlantic. With the same algorithm used in DeMaria and Kaplan (1994) and Zeng et al. (2007, 2008), an empirical MPI as an exponential function of SST, which fits the maximum intensity, can be given below:

$$V_{mpi} = A + Be^{C(SST - T_0)}. \quad (1)$$

The constants A, B, C, and T_0 in Eq. (1) are estimated using a least squares fit. The fitted curve is shown in red in Fig. 1, where $A = 27.58\,m\,s^{-1}$, $B = 74.03\,m\,s^{-1}$, $C = 0.1903°C^{-1}$, and $T_0 = 30.0°C$. The fitted MPI curve is very close to that obtained in Zeng et al. (2008) with $A = 29.5\,m\,s^{-1}$, $B = 64.6\,m\,s^{-1}$, and $C = 0.1813°C^{-1}$ but is higher than that of DeMaria and Kaplan (1994) with their constants of $28.2\,m\,s^{-1}$, $55.8\,m\,s^{-1}$, and $0.1813°C^{-1}$, respectively (see Fig. 1). The small difference between the curve obtained in this study and that

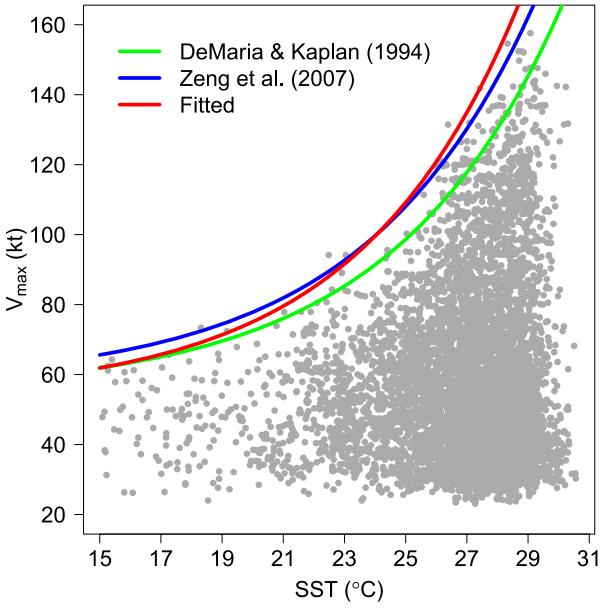

FIG. 1. Scatter diagram of intensity (maximum sustained near-surface wind speed V_{max}; kt) vs SST (°C) for all TC cases in the North Atlantic during 1988–2014. The fitted maximum potential intensity (MPI) in this study (red) is compared with the fitted MPI in DeMaria and Kaplan (1994) (green) and in Zeng et al. (2007) (blue).

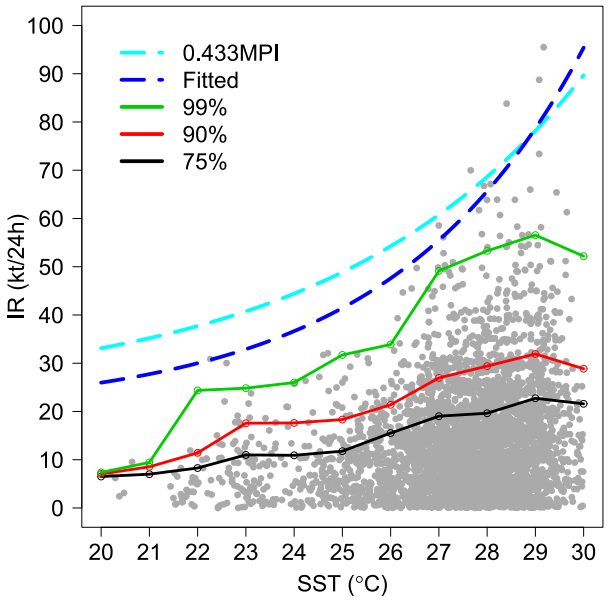

FIG. 2. Scatter diagram of IR (24-h V_{max} increase; kt) vs SST (°C) for all intensifying TC cases in the North Atlantic during 1988–2014. The 99th, 90th, and 75th percentiles for IR in each 1°C SST bin are given by the green, red, and black curves with open circles, respectively. The fitted MPIR is given by the long-dashed blue curve. The corresponding MPIR obtained from the simplified dynamical system model discussed in section 5 is shown by the dashed light blue curve.

in Zeng et al. (2007) results mainly from different time periods covered and higher-temporal- and spatial-resolution SST data used in this study. The large difference between our curve and that of DeMaria and Kaplan (1994) is likely due to the early TC best-track data and the use of climatological SST data in their study.

b. TC IR versus SST

Figure 2 shows the scatter diagram of IR versus SST for all intensifying TC cases during 1988–2014 in the North Atlantic together with the 75th, 90th, and 99th percentiles in each SST bin. Very similar to the increasing trend of TC intensity with the increase in SST, the IR shows a general increasing trend with increasing SST as well with a more rapid increasing trend when SST is higher than 27°C. The decreasing trend of IR with increasing SST for SST higher than 29°C could be due to the fact that most TCs over those high SSTs were at their formation and initial development stages. Note that TCs often experience their largest IR when they are at hurricane (30–40 m s^{-1}) intensities, as recently documented in Xu and Wang (2015). Therefore, the decreasing trend does not mean TC IR decreases with increasing SST at SST higher than 29°C. This is consistent with the distribution of TC intensity as a function of SST, which shows that the most intense TCs did not occur at the highest SSTs (Fig. 1).

Since TC intensification and maintenance of TC intensity are controlled by similar physical processes, namely the energy source for TC development and maintenance is the surface entropy flux from the underlying ocean, we can hypothesize that similar to TC intensity, there also exists an upper bound for TC IR, namely an MPIR given favorable environmental conditions in the atmosphere and the underlying ocean. Therefore, a functional relationship between SST and the MPIR can be expected. We can assume that similar to the MPI, the MPIR can also be expressed as an exponential function of SST. Based on the same fitting algorithm as used for the MPI, we obtained the fitting constants in Eq. (1) as $A = 10.17\,\mathrm{m\,s^{-1}\,day^{-1}}$, $B = 38.91\,\mathrm{m\,s^{-1}\,day^{-1}}$, $C = 0.25°\mathrm{C}^{-1}$, and $T_0 = 30°\mathrm{C}$. As we can see from Fig. 2, IRs of almost all intensifying TC cases are under the fitted curve except for four points that are larger than the fitted MPIR. Those four points all have extremely larger IRs (see their detailed information listed in Table 2). Since there are also uncertainties in determining TC intensity in the best-track data and in SST in the reanalysis data, these four points could be considered as rare cases (or related to some uncertainties) and thus were not included in our fitting. A detailed analysis on the four rare cases is needed but is reserved for a future study. Nevertheless, overall the fitted curve can provide a maximum possible IR, namely MPIR, for a given SST and should be useful for the estimation of maximum possible IR of a TC in operational forecasts.

Figure 3 and Table 1 give the probability distributions of TC IR (Fig. 3a) and the lifetime maximum IR (Fig. 3b) in each SST bin. About 86.7% of the intensifying cases occurred over SSTs higher than 26°C and only about 13.3% occurred over SSTs lower than 26°C (Table 1 and Fig. 3a). Both the averaged IR and the averaged top 50% of IRs show an increasing trend with increasing SST over

TABLE 2. Information for the four extremely high-IR TC cases. Here V_s is the lifetime maximum intensity of the given TC.

ID	Name	Time and date	Lat (°N)	Lon (°W)	V_{max} (kt)	V_s (kt)	IR (kt day^{-1})
AL2505	Wilma	0600 UTC 18 Oct 2005	15.7	79.9	60	157.6	88.8
AL2505	Wilma	1200 UTC 18 Oct 2005	16.2	80.3	65	157.6	95.5
AL0607	Felix	0000 UTC 2 Sep 2007	12.6	66.1	65	142.3	83.8
AL0908	Ike	0600 UTC 3 Sep 2008	20.2	48.8	55	119.1	70.0

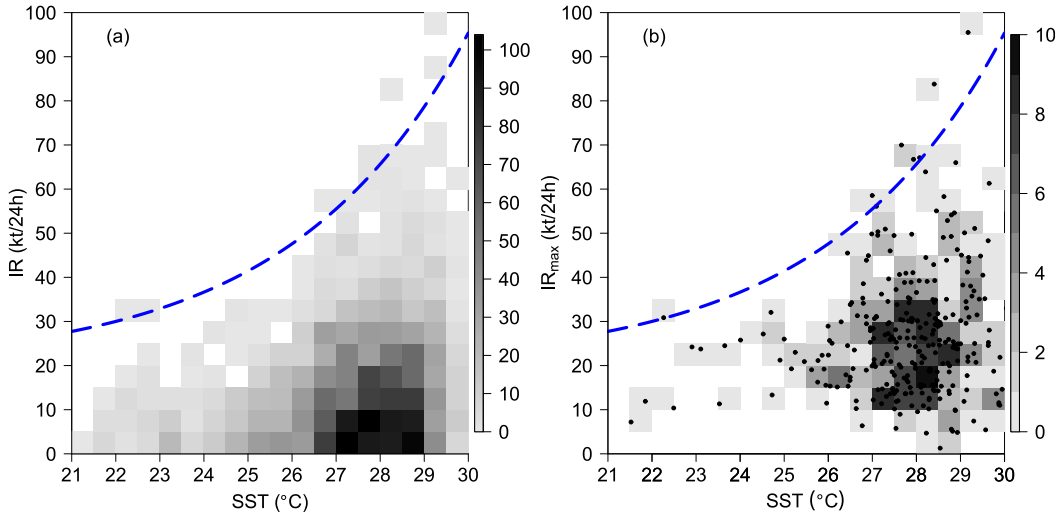

FIG. 3. (a) Frequency of TC IR (kt day^{-1}) vs SST (°C) and (b) frequency and scatter diagram of the lifetime IR$_{max}$ (kt day^{-1}) vs SST (°C). The empirically fitted MPIR (kt day^{-1}) as a function of SST (°C) as given in Fig. 2 is also shown in both (a) and (b) in dashed blue for a reference.

SSTs higher than 25°C with the latter larger than 20 knots day^{-1} (1 kt = 0.51 m s^{-1}) over SSTs above 27°C. This suggests that large IR cases mostly occurred with high SST. Consistently, over 88.9% of the lifetime maximum IRs (IR$_{max}$) occurred over SSTs higher than 26°C and about 79.0% of IR$_{max}$ occurred over SSTs above 27°C (Table 1 and Fig. 3b). This strongly suggests that, similar to the MPI, the TC IR and the MPIR is largely controlled by the underlying SST.

To further examine the relationship between the lifetime IR$_{max}$ and SST, we also analyzed the geographical distribution of the lifetime IR$_{max}$ and climatological SST. Figure 4 shows the spatial distributions of climatological SST (averaged in June–October during 1988–2014) and the location of each TC at the time of its IR$_{max}$ and the corresponding value of the lifetime IR$_{max}$. Note that the distribution of IR$_{max}$ is considerably smoothed to give an overview of the spatial pattern with the smoothing algorithm of a two-dimensional surface fitting as described in Xu and Wang (2015). There is a tendency for more TCs to reach their lifetime IR$_{max}$ over higher SSTs and, in particular, in a zonally elongated tropical belt along 10°–15°N, the west-central North Atlantic, the Caribbean Sea, and the Gulf of Mexico. There are two areas with large IR$_{max}$. One is centered at around 18°N, 50°W over the central North Atlantic and the other one is in the area 10°–20°N, 60°–90°W over the southern Caribbean Sea. The smoothed IR$_{max}$ over these areas is generally larger than 30 kt day^{-1}; that is, it satisfied the rapid intensification (RI) criterion (Kaplan et al. 2010). Note that large values of the lifetime IR$_{max}$ are not always correlated with SST, in particular for the large IR$_{max}$ area over the central North Atlantic. Nevertheless, the number of cases reaching their lifetime IR$_{max}$ is relatively low partially because of the relatively lower SSTs and the effect of other large-scale atmospheric conditions as discussed below.

It is well known that in addition to SST, the TC IR can be largely affected by both the large-scale atmospheric environment, such as VWS, and the internal dynamics, such as the concentric eyewall cycle (Wang and Wu 2004; Wang 2012). Here, to understand the spatial distribution of the lifetime IR$_{max}$ and SST shown in Fig. 4a, we examined the spatial distribution of the VWS between 200 and 850 hPa averaged within a radius of 1000 km from the center of each TC at the time of its lifetime IR$_{max}$ with the results shown in Fig. 4b. Note that the smoothing algorithm as applied to the lifetime IR$_{max}$ was also applied to VWS analysis so that the overall pattern can be easily visualized. Comparing Fig. 4b with Fig. 4a, we can see that very few TCs reached their lifetime IR$_{max}$ and relatively low IR$_{max}$ occurred in regions with VWS larger than 10 m s^{-1} while most TCs reached their lifetime IR$_{max}$ over high SST and low VWS, especially for those TCs with large IR$_{max}$. This strongly suggests that both SST and VWS are key factors that determine the IR of a TC.

c. *Relative intensification rate (RIR)*

As already seen from Figs. 2 and 3, both the IR and the lifetime IR$_{max}$ of TCs were well below their MPIR. This is because the MPIR is mainly determined by SST and gives

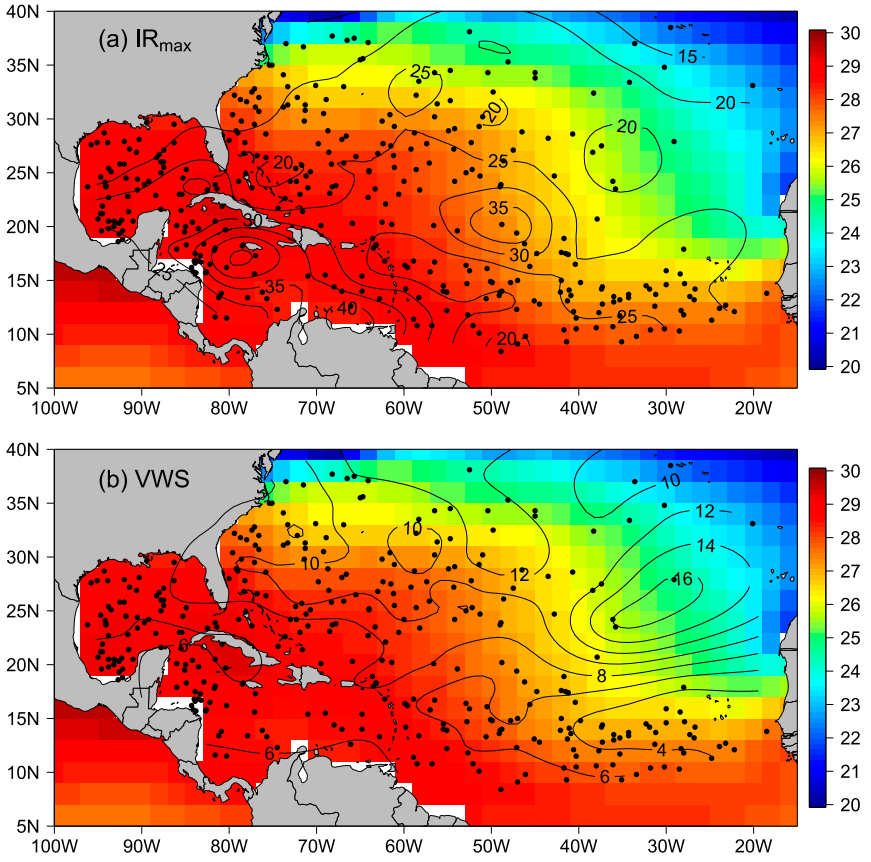

FIG. 4. Locations of each storm at the time of its lifetime maximum IR (dots) and the climatological SST averaged during June–October between 1988 and 2014 (°C; colored shading) overlapped with (a) the lifetime maximum IR (kt day^{-1}; contours) and (b) the environmental VWS (m s^{-1}) between 200 and 850 hPa averaged within 1000-km radius from the center of each TC at the time of its lifetime maximum IR (contours).

the upper bound of the IR of a TC. In reality, in addition to SST, the IR of a TC is often affected by both large-scale VWS and internal dynamics as mentioned above. In this section, similar to the analysis for the frequency and cumulative frequency distributions of relative intensity conducted by DeMaria and Kaplan (1994), we analyzed the frequency and cumulative frequency distributions of the relative IR (IR/MPIR) and relative lifetime IR_{max} (IR_{max}/MPIR). The RIR and lifetime RIR_{max} are defined as the IR and IR_{max} normalized by the corresponding MPIR at the given time, respectively.

Figure 5 shows the RIR and RIR_{max} distributions (Fig. 5a) and their corresponding cumulative distributions (Fig. 5b) for all intensifying TC cases and TCs, respectively, during 1988–2014 over the North Atlantic. We can see that very few TCs reached their MPIR even when they were at their lifetime IR_{max} (Fig. 5a). The peak (30.3%) in the frequency distribution of RIR was at 10% and the second peak (25.0%) was at 20% (green bars in Fig. 5a). The percentage in the distribution decreases rapidly as the RIR increases. For example, 7.2% was at 50% and 3.5% was at 60% and became rare for RIR larger than 70%. The frequency distribution of the lifetime RIR_{max} shows a quite different pattern (red bars in Fig. 5a) from that of the RIR. The peak of 18.8% in the distribution was at 30% and 40% of the RIR_{max} and 18.2% occurred at 50% of the RIR_{max}. Compared with the percentage of RIR cases, more cases were on the high RIR_{max} side. These differences should not be surprising since the RIR_{max} was based on choosing the maximum IR.

The above features can be easily seen from the cumulative distributions of the RIR and the lifetime RIR_{max} shown in Fig. 5b. Only a small portion of the intensifying TC cases reached their MPIR. For example, about 46% of the intensifying cases reached 20% of their MPIR. Only 26% reached 30% of their MPIR, but only 14% (6%) reached 40% (50%) of their MPIR (green curve in Fig. 5b). Nevertheless, the cumulative distribution of the lifetime RIR_{max} shifted considerably to the right, namely on the higher RIR_{max}

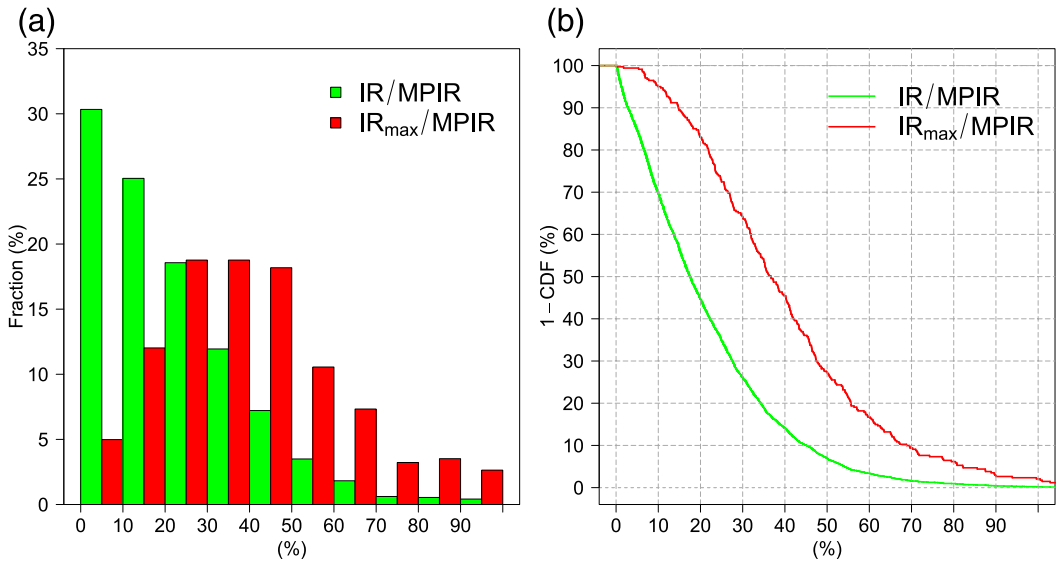

FIG. 5. (a) The probability distribution (%) of the relative IR (green bars) and the relative lifetime IR_{max} (red) for all intensifying TC cases over the North Atlantic during 1988–2014 stratified in 10% bins and (b) the cumulative distribution function (1 − CDF) of relative IR and relative lifetime IR_{max}. The relative IR (IR_{max}) is defined as the IR (IR_{max}) normalized by the MPIR at the given time.

side. About 64% of IR_{max} reached 30% of their MPIR and 28% (17%) reached 50% (60%) of their MPIR, but only 7% of IR_{max} reached 80% of their MPIR (red curve in Fig. 5b).

Figure 6 shows the location of each TC at the time of its lifetime RIR_{max} and the spatial distribution of the smoothed lifetime RIR_{max} with climatological SST shown as the background. The spatial distribution of the lifetime RIR_{max} shows a very similar pattern to that of the IR_{max} shown in Fig. 4a. Note that values larger than 40% for RIR_{max} were in regions with high SST and low VWS (Fig. 4b). In particular, given the SST, VWS seems to contribute largely to the lifetime RIR_{max}. Note that the high values of lifetime RIR_{max} over low SST north of 30°N were not representative since the small number of cases and the fitted observed MPIR may be underestimated because of relatively large VWS in the midlatitude westerlies in the basin.

4. SST dependence of maximum IR in a simplified dynamical system

Xu and Wang (2015) explained the observed intensity dependence of TC IR over the North Atlantic based on the simplified dynamical system model for TC intensity prediction developed by DeMaria (2009). They showed from observations that the maximum IR often occurs at intermediate intensity of 30–40 m s^{-1}. Although the simplified dynamical system model was developed based on a logistic growth equation (LGE), it shows good skill in predicting TC intensity change and is still used in National Hurricane Center (NHC) as one of the major forecast members in ensemble TC intensity prediction (M. DeMaria 2016, personal communication). This implies that the dynamical system model captures the major physical and dynamical processes of TC intensification. Similar to Xu and Wang (2015), here we examine the SST dependence of the MPIR constructed based on observations as discussed in section 3 in the simplified dynamical system model of DeMaria (2009).

The equation of the simplified dynamical system model [Eq. (3) in DeMaria 2009] is given as

$$\mathrm{IR} = \frac{dV_{\max}}{dt} = \kappa V_{\max} - \beta V_{\max}\left(\frac{V_{\max}}{V_{\mathrm{mpi}}}\right)^{n}, \qquad (2)$$

where V_{max} is the time-dependent maximum sustained near-surface wind speed. The IR ($=dV_{max}/dt$) is determined by a growth term and a term that limits the maximum wind speed to the MPI in terms of the maximum surface wind speed V_{mpi}, which can be calculated from the underlying SST on the storm track, κ is the growth rate, and β and n are positive constants that determine how rapidly and how close the solution for V_{max} can come to V_{mpi}. DeMaria (2009) found the values for β and n of 1 day^{-1} and 2.5, respectively, based on the regression analysis using historical best-track data for North Atlantic TCs.

By letting $\partial \mathrm{IR}/\partial V_{\max} = 0$ in Eq. (2), Xu and Wang (2015) found that IR reaches a maximum value when the

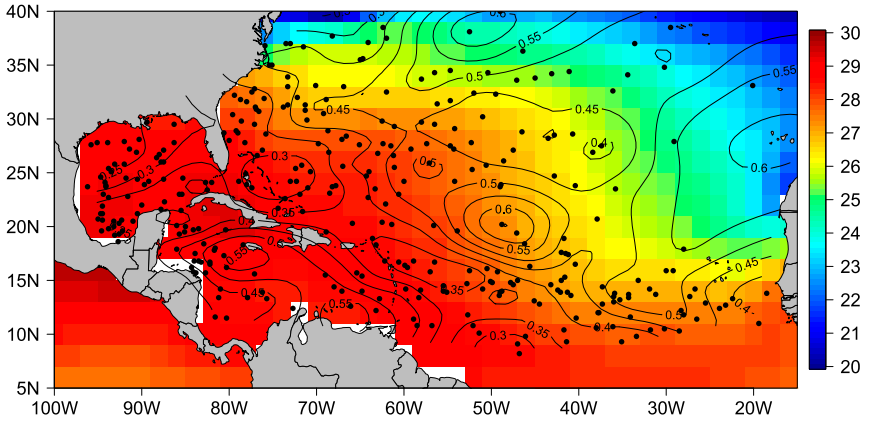

FIG. 6. As in Fig. 4a, but overlaid with the lifetime relative IR_{max} (contours).

storm intensity is around $V_{max} = V|_{mpir}$ (for a given V_{mpi}, or equivalently a given SST)

$$V|_{mpir} = V_{mpi}\left[\frac{\kappa}{(n+1)\beta}\right]^{1/n}. \tag{3}$$

Replacing V_{max} in Eq. (2) with $V|_{mpir}$ in Eq. (3), we can get the expression for the maximum IR (IR_{max}) for a given V_{mpi} or SST as

$$IR_{max} = \kappa V_{mpi}\left(\frac{n}{n+1}\right)\left[\frac{\kappa}{(n+1)\beta}\right]^{1/n}. \tag{4}$$

To determine IR_{max}, we need to know the growth rate κ in Eq. (4). In real-time forecast, DeMaria (2009) estimated κ using the IR in previous 24 h. Here we are interested in the MPIR. Namely, we assume that the TC would reach its MPI given favorable environmental conditions. In this case, for a given SST, the TC has its MPI V_{mpi}. Letting $dV_{max}/dt = 0$ and $V_{max} = V_{mpi}$ in Eq. (2), we can obtain $\kappa = \beta$ and Eq. (4) then becomes

$$MPIR = \beta V_{mpi}\left(\frac{n}{n+1}\right)\left[\frac{1}{(n+1)}\right]^{1/n}. \tag{5}$$

Using $n = 2.5$ and $\beta = (24\,\text{h})^{-1}$, we can have

$$MPIR = 0.433 V_{mpi}\,\text{day}^{-1}, \tag{6}$$

and the corresponding V_{mpir} can be given as

$$V_{mpir} = V_{mpi}(n+1)^{-1/n} \approx 0.606 V_{mpi}. \tag{7}$$

Equation (7) is similar to that in Xu and Wang (2015) except that the lifetime maximum intensity of the observed TC V_s is replaced by V_{mpi} here. This is because here we assumed the TC reaches its MPI.

As a rough comparison, we plot in Fig. 2 the MPIR curve from Eq. (6) using the fitted MPI given in Fig. 1. The MPIR from the simplified dynamical system model is comparable to that obtained directly from observations and also shows a nonlinear increasing trend with SST. However, the former shows a smaller slope than the latter—namely, the MPIR from the simplified dynamical system model is higher on the low-SST side and a little bit lower on the high-SST side than the one obtained from the observationally fitted MPIR. This difference can be explained by the fact that the fitted MPIR from observations has included the effect of VWS over low SSTs because VWS is often large over the low-SST region in the higher latitudes. Therefore, it is reasonable to consider that the fitted MPIR underestimated the "theoretical" MPIR, in particular in the regions with low SST where VWS is often large.

5. Conclusions

In this study, the relationship between SST and IR of TCs over the North Atlantic was examined based on the best-track TC data and the observed SST during 1988–2014. Among all intensifying TC cases studied, about 86.7% occurred over SST higher than 26°C. Both the averaged IR of all intensifying cases and the averaged IR of the top 50% IRs show an increasing trend with increasing SST, with the latter being larger than 20 kt day^{-1} over SSTs higher than 27°C. Consistently, over 88.9% of the lifetime maximum IRs (IR_{max}) occurred over SSTs higher than 26°C and about 79% of the lifetime IR_{max} occurred over SSTs higher than 27°C. Overall, the TC IR increases with increasing SST but the increasing trend becomes more rapid when SST is higher than 27°C.

Considering the fact that TC intensification and maintenance of TC intensity are controlled by similar physical

processes—namely, the energy source for TC development and maintenance is the surface entropy flux from the underlying ocean—we hypothesized that similar to TC intensity, there also exists an upper bound for TC IR, namely the MPIR given favorable environmental conditions. This motivated us to construct an empirical relationship between SST and the MPIR of TCs based on observations. Similar to the empirical relationship between SST and the TC MPI previously developed, the TC MPIR developed in this study is a function of SST and shows a nonlinear increasing trend with increasing SST. The dependence of lightning frequency in TCs on SST documented in Stevenson et al. (2016) seems to support our results since the TC intensification, in particular the rapid intensification, is often accompanied with an increase in flash count. Stevenson et al. (2016) showed that the lightning frequency within a radius of 300 km in TCs over both the eastern Pacific and North Atlantic increases rapidly with SST when SST is higher than 26°C (see their Fig. 4).

Further analysis for the lifetime IR_{max} of each TC indicates that in addition to SST, TC IR is considerably modulated by the large-scale environmental VWS. Results show that very few TCs reached their MPIR and in general only low values of IR_{max} occurred in regions with VWS larger than 10 m s^{-1} while most TCs reached their lifetime IR_{max} over high SST and low VWS, especially for those TCs with large IR_{max} or for TCs experiencing RI. Based on the MPIR, the relative IR (RIR) and the lifetime maximum RIR (RIR_{max}) were analyzed. Results show that only 14% (7%) of intensifying TC cases reached 40% (50%) of their MPIR. About 28% (17%) of TCs reached 50% (60%) of their lifetime MPIR, and only 7% reached 80% of their MPIR at the time when they were at their lifetime IR_{max}. An examination of the geographical distribution of RIR_{max} indicates that RIR_{max} larger than 40% were in regions with high SST and low VWS.

The relationship between SST and the MPIR in the simplified dynamical system model previously developed for TC intensity prediction by DeMaria (2009) has also been examined. Although some discrepancies exist, in particular in regions with relatively low SSTs where the large-scale VWS is generally large, the relationship obtained from the simplified dynamical system model is very similar to that obtained from the observational fitting. Our results thus provide an additional observational support to the intensity prediction scheme based on the simplified dynamical system model from a different perspective.

Similar to the MPI, the MPIR, which is mainly controlled by the underlying SST, provides a good approximation to the upper bound of IR of a TC. Note that in addition to SST, which is critical to surface enthalpy flux under the eyewall of a TC, the theoretical E-MPI also depends on the outflow-layer temperature, which together with SST determines the thermodynamic efficiency of the TC system (Emanuel 1988, 1991, 1995, 1997). Zeng et al. (2008) showed that the outflow-layer temperature and thus the thermodynamic efficiency depend almost linearly on SST (see their Figs. 2a and 2b). Therefore, it is not surprising that the MPIR (similar to the MPI) can be mainly determined by the underlying SST alone. In addition, similar to the MPI theory, although the IR of a TC always involves complex internal dynamics, the MPIR is subject to well-organized TCs with all favorable internal dynamics [as inferred from results in Xu and Wang (2015)]. As a result, no detailed internal dynamics is explicitly required in determining the MPIR.

As the first effort, the possible effects of atmospheric conditions and the upper-ocean processes on TC IR have not been considered in this study because we focused on the maximum possible IR. Nevertheless, since the functional relationship between SST and the MPIR has been obtained based on the long-term observational fitting, it would give a reliable upper bound of IR of a real TC over the North Atlantic. Furthermore, this study provides the observational evidence for the existence of the MPIR, suggesting that a physically based MPIR theory could be developed in a future study.

Acknowledgments. This study has been supported in part by the National Basic Research Program of China (973 Program) under Contract 2015CB452805 and National Natural Science Foundation of China under Grant 411309634 and in part by the NSF Grant AGS-1326524. Additional support has been provided by a JAMSTEC grant to the University of Hawai'i at Mānoa.

REFERENCES

Chen, X., Y. Wang, and K. Zhao, 2015: Synoptic flow patterns and large-scale characteristics associated with rapidly intensifying tropical cyclones in the South China Sea. *Mon. Wea. Rev.*, **143**, 64–87, doi:10.1175/MWR-D-13-00338.1.

DeMaria, M., 2009: A simplified dynamical system for tropical cyclone intensity prediction. *Mon. Wea. Rev.*, **137**, 68–82, doi:10.1175/2008MWR2513.1.

——, and J. Kaplan, 1994: Sea surface temperature and the maximum intensity of Atlantic tropical cyclones. *J. Climate*, **7**, 1324–1334, doi:10.1175/1520-0442(1994)007<1324:SSTATM>2.0.CO;2.

——, M. Mainelli, L. K. Shay, J. A. Knaff, and J. Kaplan, 2005: Further improvements in the Statistical Hurricane Intensity Prediction Scheme (SHIPS). *Wea. Forecasting*, **20**, 531–543, doi:10.1175/WAF862.1.

Emanuel, K. A., 1986: An air–sea interaction theory of tropical cyclones. Part I: Steady-state maintenance. *J. Atmos. Sci.*, **43**, 585–604, doi:10.1175/1520-0469(1986)043<0585:AASITF>2.0.CO;2.

——, 1988: The maximum intensity of hurricanes. *J. Atmos. Sci.*, **45**, 1143–1155, doi:10.1175/1520-0469(1988)045<1143:TMIOH>2.0.CO;2.

——, 1991: The theory of hurricanes. *Annu. Rev. Fluid Mech.*, **23**, 179–196, doi:10.1146/annurev.fl.23.010191.001143.

——, 1995: The behavior of a simple hurricane model using a convective scheme based on subcloud-layer entropy equilibrium. *J. Atmos. Sci.*, **52**, 3960–3968, doi:10.1175/1520-0469(1995)052<3960:TBOASH>2.0.CO;2.

——, 1997: Some aspects of hurricane inner-core dynamics and energetics. *J. Atmos. Sci.*, **54**, 1014–1026, doi:10.1175/1520-0469(1997)054<1014:SAOHIC>2.0.CO;2.

——, C. DesAutels, C. Holloway, and R. Korty, 2004: Environmental control of tropical cyclone intensity. *J. Atmos. Sci.*, **61**, 843–858, doi:10.1175/1520-0469(2004)061<0843:ECOTCI>2.0.CO;2.

Gray, W. M., 1968: Global view of the origin of tropical disturbances and storms. *Mon. Wea. Rev.*, **96**, 669–700, doi:10.1175/1520-0493(1968)096<0669:GVOTOO>2.0.CO;2.

Holland, G. J., 1997: The maximum potential intensity of tropical cyclones. *J. Atmos. Sci.*, **54**, 2519–2541, doi:10.1175/1520-0469(1997)054<2519:TMPIOT>2.0.CO;2.

Kaplan, J., M. DeMaria, and J. A. Knaff, 2010: A revised tropical cyclone rapid intensification index for the Atlantic and eastern North Pacific basins. *Wea. Forecasting*, **25**, 220–241, doi:10.1175/2009WAF2222280.1.

Kleinschmidt, E., Jr., 1951: Grundlagen einer Theorie der tropischen Zyklonen. *Arch. Meteor. Geophys. Bioklimatol.*, **4A**, 53–72, doi:10.1007/BF02246793.

Kurihara, Y., M. A. Bender, and R. J. Ross, 1993: An initialization scheme of hurricane models by vortex specification. *Mon. Wea. Rev.*, **121**, 2030–2045, doi:10.1175/1520-0493(1993)121<2030:AISOHM>2.0.CO;2.

Malkus, J. S., and H. Riehl, 1960: On the dynamics and energy transformations in steady-state hurricane. *Tellus*, **12**, 1–20, doi:10.1111/j.2153-3490.1960.tb01279.x.

Merrill, R. T., 1988: Environmental influences on hurricane intensification. *J. Atmos. Sci.*, **45**, 1678–1687, doi:10.1175/1520-0469(1988)045<1678:EIOHI>2.0.CO;2.

Miller, B. I., 1958: On the maximum intensity of hurricanes. *J. Meteor.*, **15**, 184–195, doi:10.1175/1520-0469(1958)015<0184:OTMIOH>2.0.CO;2.

Murakami, H., and Coauthors, 2015: Simulation and prediction of category 4 and 5 hurricanes in the high-resolution GFDL HiFLOR coupled climate model. *J. Climate*, **28**, 9058–9079, doi:10.1175/JCLI-D-15-0216.1.

Reynolds, R. W., N. A. Rayner, T. M. Smith, D. C. Stokes, and W. Wang, 2002: An improved in situ and satellite SST analysis for climate. *J. Climate*, **15**, 1609–1625, doi:10.1175/1520-0442(2002)015<1609:AIISAS>2.0.CO;2.

——, T. M. Smith, C. Liu, D. B. Chelton, K. S. Casey, and M. G. Schlax, 2007: Daily high-resolution-blended analyses for sea surface temperature. *J. Climate*, **20**, 5473–5496, doi:10.1175/2007JCLI1824.1.

Stevenson, S. N., K. L. Corbosiero, and S. F. Abarca, 2016: Lightning in eastern North Pacific tropical cyclones: A comparison to the North Atlantic. *Mon. Wea. Rev.*, **144**, 225–239, doi:10.1175/MWR-D-15-0276.1.

Wang, Y., 2012: Recent research progress on tropical cyclone structure and intensity. *Trop. Cyclone Res. Rev.*, **1**, 254–275.

——, and C.-C. Wu, 2004: Current understanding of tropical cyclone structure and intensity changes—A review. *Meteor. Atmos. Phys.*, **87**, 257–278, doi:10.1007/s00703-003-0055-6.

——, Y. Rao, Z.-M. Tan, and D. Schönemann, 2015: A statistical analysis of the effects of vertical wind shear on tropical cyclone intensity change over the western North Pacific. *Mon. Wea. Rev.*, **143**, 3434–3453, doi:10.1175/MWR-D-15-0049.1.

Xu, J., and Y. Wang, 2015: A statistical analysis on the dependence of tropical cyclone intensification rate on the storm intensity and size in the North Atlantic. *Wea. Forecasting*, **30**, 692–701, doi:10.1175/WAF-D-14-00141.1.

Zeng, Z., Y. Wang, and C.-C. Wu, 2007: Environmental dynamical control of tropical cyclone intensity—An observational study. *Mon. Wea. Rev.*, **135**, 38–59, doi:10.1175/MWR3278.1.

——, L.-S. Chen, and Y. Wang, 2008: An observational study of environmental dynamical control of tropical cyclone intensity in the North Atlantic. *Mon. Wea. Rev.*, **136**, 3307–3322, doi:10.1175/2008MWR2388.1.